

See discussions, stats, and author profiles for this publication at: <https://www.researchgate.net/publication/236210060>

New molecular scaffolds for the design of Alzheimer's acetylcholinesterase inhibitors identified using ligand- and receptor-based virtual screening

ARTICLE *in* MEDICINAL CHEMISTRY RESEARCH · APRIL 2013

Impact Factor: 1.4 · DOI: 10.1007/s00044-012-0227-3

CITATIONS

9

READS

49

4 AUTHORS, INCLUDING:



Nitin Chitranshi

Macquarie University

16 PUBLICATIONS 27 CITATIONS

SEE PROFILE



Shipra Gupta

Indian Institute of Science Education and R...

14 PUBLICATIONS 41 CITATIONS

SEE PROFILE



Prahlad Seth

Biotech Park Lucknow

294 PUBLICATIONS 4,991 CITATIONS

SEE PROFILE

New molecular scaffolds for the design of Alzheimer's acetylcholinesterase inhibitors identified using ligand- and receptor-based virtual screening

**Nitin Chitranshi, Shipra Gupta,
Pushpendra Kumar Tripathi & Prahlad
Kishore Seth**

Medicinal Chemistry Research

ISSN 1054-2523

Med Chem Res

DOI 10.1007/s00044-012-0227-3



Your article is protected by copyright and all rights are held exclusively by Springer Science+Business Media, LLC. This e-offprint is for personal use only and shall not be self-archived in electronic repositories. If you wish to self-archive your work, please use the accepted author's version for posting to your own website or your institution's repository. You may further deposit the accepted author's version on a funder's repository at a funder's request, provided it is not made publicly available until 12 months after publication.

New molecular scaffolds for the design of Alzheimer's acetylcholinesterase inhibitors identified using ligand- and receptor-based virtual screening

Nitin Chitranshi · Shipra Gupta ·
Pushpendra Kumar Tripathi ·
Prahlaad Kishore Seth

Received: 14 May 2012 / Accepted: 5 September 2012
© Springer Science+Business Media, LLC 2012

Abstract The identification of important chemical features of acetylcholinesterase (AChE) inhibitors will be helpful to discover the potent candidate to inhibit the AChE activity. The best hypothesis from structure-based, Hypo1, one hydrophobic (H) pointed toward ILE444, TRP84, three hydrogen bond acceptor (HBA), two hydrogen bond donor, one positive ionizable toward TRP84, PHE330, and 11 excluded volume sphere, were generated using Ligand-Scout. Test and decoy sets were used to corroborate the best hypotheses, and the validated hypotheses were used to screen the Maybridge database. Only 14 compounds were prioritized as promising hits. The quantitative structure–activity relationship (QSAR) equation was developed based on 44 AChE inhibitors: 34 training set compounds and 10 test set compounds. The model was developed using five information-rich descriptors—HBA, log *P*, HOF, EE, and dipole—playing an important role in determining AChE inhibitory activity. QSAR model (model 3) yielded good statistical data, $r^2 = 0.723$; $q^2 = 0.703$; $n = 34$ for training set. This model was further validated using leave-one-out cross-validation approach, Fischer statistics (*F*), *Y* randomisation test, and prediction based on the test data set. Molecular docking of 44 1-indanone derivatives &

screened hits compounds were performed to identify the binding residue in AChE. Finally, the screened hits prioritized belong to several classes of molecular scaffolds with several available substitution positions that could allow chemical modification to enhance AChE binding affinity for Alzheimer disease.

Keywords Acetylcholinesterase (AChE) · 3D Pharmacophore · 2D Descriptors · Molecular docking · QSAR · Binding site

Introduction

Alzheimer's disease (AD) is an age-related neurodegenerative disease, and the most frequent and predominant cause of dementia in the elderly, provoking progressive cognitive decline, psychobehavior disturbances, memory loss, the presence of senile plaques, neurofibrillary tangles, and the decrease in cholinergic transmission (Parihar and Hemnani, 2004; Scarpini *et al.*, 2003). It is well known that two forms of cholinesterases coexist ubiquitously throughout the body, i.e., acetylcholinesterase (AChE) and butyrylcholinesterase (BChE). They catalyze the degradation of the neurotransmitter acetylcholine, leading to the termination of cholinergic neurotransmission (Nachon *et al.*, 2005; Silman and Sussman, 2005). Cholinesterase inhibitors (ChEI) represent the treatment of choice for AD (Rodriguez-Franco *et al.*, 2005; Shen *et al.*, 2005). AChE has a well-established esterase activity. The pharmacological role of BChE is not yet completely understood. BChE may have a compensatory role in the modulation of the hydrolysis of acetylcholine (ACh) in brain with degenerative changes. Consequently, BChE may be target for increasing the cholinergic tone in AD patients (Giacobini *et al.*, 2002; Greig *et al.*, 2001).

Electronic supplementary material The online version of this article (doi:10.1007/s00044-012-0227-3) contains supplementary material, which is available to authorized users.

N. Chitranshi (✉) · P. K. Tripathi
Department of Pharmacy, Rameshwaram Institute of
Technology & Management, Gautam Buddha Technical
University, Lucknow 227202, Uttar Pradesh, India
e-mail: nitin0916@gmail.com

S. Gupta · P. K. Seth
Bioinformatics Centre, Biotech Park, Sector-G, Jankipuram,
Lucknow 226021, Uttar Pradesh, India

Many efforts have been made in the search for potent AChE inhibitors, and a large number of naturally occurring and synthetic AChE inhibitors have already been reported (Bolognesi *et al.*, 2005; Savini *et al.*, 2003). Among them, four representative anti-AChE agents, tacrine, rivastigmine, donepezil, and galanthamine, have been approved by FDA for the treatment of AD (Allen and Burns, 1995; Francis *et al.*, 1999; Ibach and Haen, 2004). The 3-D structure of AChE from native *Torpedo californica* (TcAChE) has been determined by X-ray crystallography (Protein Data Bank, PDB code: 2ACE) (Raves *et al.*, 1997). There are also lot of other complex structures of TcAChE with inhibitors determined experimentally, such as donepezil (PDB code: 1EVE) (Kryger *et al.*, 1999), tacrine (PDB code: 1ACJ) (Harel *et al.*, 1993), decamethonium ion (PDB code: 1ACL) (Harel *et al.*, 1993), *m*-(3*N*-trimethylammonio) trifluoroacetophen-one (PDB code: 1AMN) (Harel *et al.*, 1996), huperzine A (PDB code: 1VOT) (Raves *et al.*, 1997), galanthamine (PDB code: 1DX6) (Greenblatt *et al.*, 1999), rivastigmine (PDB code: 1GQR) (Bar-On *et al.*, 2002) and edrophonium (PDB code: 2ACK) (Ravelli *et al.*, 1998). All these significantly enhance our understanding of the structural elements of AChE. The binding pocket of AChE is a long and narrow region which consists of two separated ligand binding sites: the catalytic (central) site and the peripheral anionic site (Kryger *et al.*, 1999; Raves *et al.*, 1997). The catalytic site is the binding site of classical AChE inhibitors, such as tacrine and huperzine A, which has been studied thoroughly. On the other side, the function of the peripheral site has not been elucidated clearly as yet. Recent studies have demonstrated that the peripheral site might accelerate the aggregation and deposition of beta-amyloid peptide, which is considered as another cause of AD (Bartolini *et al.*, 2003; Inestrosa *et al.*, 1996; Silman and Sussman, 2005). Therefore, it is an ideal AChE inhibitor should bind to the catalytic and peripheral sites simultaneously, which could disrupt the interactions between the enzyme and the beta-amyloid peptide, and hence slow down the progression of the disease (Du and Carlier, 2004; Munoz-Muriedas *et al.*, 2004).

Among the AChE inhibitors, donepezil, and rivastigmine are usually used early to moderate stages of AD patients to treat cognitive loss. For example, recent clinical studies showed that tacrine had hepatotoxic liability (Galisteo *et al.*, 2000), donepezil can lead diarrhea, and rivastigmine can cause vomiting. Therefore, it is urgent to identify and develop AChE inhibitors to treat AD (Du and Carlier, 2004; Munoz-Muriedas *et al.*, 2004). From the crystal structure (PDB: 1EVE), it is clear that the 5,6-dimethoxy-1-indanone moiety and benzyl piperidine moiety of donepezil interact with the peripheral and catalytic binding site of AChE, respectively (Kryger *et al.*, 1999), whereas rivastigmine is the catalytic site-binding inhibitor (Soreq and Seidman, 2001). Therefore, the catalytic and peripheral binding characteristic of the two

inhibitors, Sheng *et al.* reported a new kind of AChE inhibitors 2-substituted 5,6-dimethoxy-1-indanone derivatives, which have exhibited good inhibitory activities of AChE in vitro (Sheng *et al.*, 2005). These compounds consist of three functional groups: a 5,6-dimethoxy-1-indanone, a benzene ring, and protonated nitrogen (Table 1). The first moiety extracted from donepezil, is supposed to interact with the peripheral binding site, while the other two moieties, derived from rivastigmine (Table 1), might be able to interact with the catalytic binding site (Sheng *et al.*, 2005).

In this context, we have chosen the sequential combination of ligand similarity, pharmacophore features, molecular docking strategies, and Quantitative structure–activity relationship (QSAR) in a single workflow to obtain novel hits. The fact that these methods, when used individually, focus only on one part of the structural information available has recently prompted the development of hybrid ligand- and receptor-based virtual screening methods. These hybrid methods aim at fully exploiting all the structural information present in ligand-bound protein structures, both from the protein and ligand perspective. Although any single approach either ligand-based approaches such as QSAR or 3D pharmacophore or structure-based approach like molecular docking can be used to design new compounds but better results can be achieved using the consensus of both ligand- and structure-based design approaches.

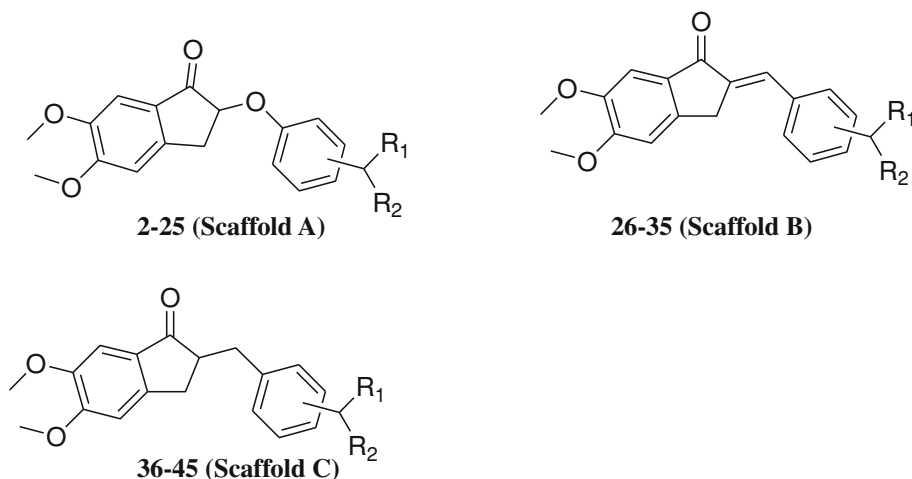
The aim of our study was to screen a possibly diverse set of small molecular structures, to obtain scaffolds capable of fitting into AChE catalytic and peripheral binding site. We performed sequential virtual screening by means of 3D pharmacophore search and virtual screening hit prioritization using molecular docking, and QSAR. Such a method allows combining receptor-based and ligand-based approaches, thus utilizing most of the currently available structural data. The novelty of this approach lies in the sequential combination of ligand (3D pharmacophore) and structure-based virtual screening facilitated through the prediction of hit compounds activity using quantitative structure activity relationship for screening against the AChE. Another important feature of this computational approach is the enhancement of its predictive power that can be used to discriminate actives from inactive in a retrospective virtual analysis. We believe that these approaches can be integrated in prospective virtual analysis to select candidates for the rational design of AChE inhibitors.

Computational methods

Dataset

The dataset of 44 1-indanone derivatives was collected from the literature (Sheng *et al.*, 2005). The dataset

Table 1 Structure, biological activities, and predicted activities of donepezil and 44 1-indanone derivatives as AChE inhibitors



Compound	R ₁	R ₂	Position of	Scaffold	IC ₅₀ (μmol/L)	pIC ₅₀		Residual
						Actual	Predicted	
Donepezil (1)					0.016	7.80		
2		H	Meta	A	1.1	5.96	5.49	0.47
3*		CH ₃		A	0.82	6.09	6.32	-0.23
4		H	Para	A	0.21	6.68	6.13	0.55
5		CH ₃		A	0.15	6.82	6.69	0.13
6*		H	Meta	A	2.28	5.64	5.42	0.22
7*		CH ₃		A	1.36	5.87	5.66	0.21
8		H	Para	A	0.1	7	6.63	0.37
9		CH ₃		A	0.22	6.66	7.04	-0.38
10		H	Meta	A	2.66	5.58	5.79	-0.21
11		CH ₃		A	1.96	5.71	6.12	-0.41
12*		H	Para	A	0.05	7.3	6.9	0.40
13		CH ₃		A	0.14	6.85	6.04	0.81
14		H	Meta	A	3.18	5.5	5.57	-0.07
15		CH ₃		A	3.58	5.45	5.28	0.17
16*		H	Para	A	0.15	6.82	6.79	0.03
17*		CH ₃		A	0.13	6.89	6.55	0.34
18		H	Meta	A	14.6	4.84	5.19	-0.35
19		CH ₃		A	22.1	4.66	4.81	-0.15
20*		H	Para	A	1.3	5.89	5.93	-0.04
21		CH ₃		A	3.14	5.5	5.44	0.06
22		H	Meta	A	6.41	5.19	5.53	-0.34
23		CH ₃		A	17.6	4.75	5.31	-0.56
24		H	Para	A	1.42	5.85	5.42	0.43
25		CH ₃		A	2.98	5.53	5.5	0.03

Table 1 continued

Compound	R1	R2	Position of	Scaffold	IC ₅₀ ($\mu\text{mol/L}$)	pIC ₅₀		Residual
						Actual	Predicted	
26*		H	Meta	B	2.14	5.67	5.45	0.22
27		H	Para	B	0.415	6.38	6.78	-0.4
28		H	Meta	B	0.487	6.31	6.5	-0.19
29*		H	Para	B	0.266	6.58	6.47	0.11
30		H	Meta	B	0.444	6.35	6.67	-0.32
31		H	Para	B	0.035	7.46	6.82	0.64
32		H	Meta	B	0.237	6.63	6.83	-0.2
33		H	Para	B	0.045	7.35	6.84	0.51
34		H	Meta	B	0.162	6.79	6.88	-0.09
35		H	Para	B	0.102	6.99	6.71	0.28
36		H	Meta	C	3.74	5.43	5.96	-0.53
37		H	Para	C	1.38	5.86	6.37	-0.51
38		H	Meta	C	0.685	6.16	6.6	-0.44
39		H	Para	C	0.38	6.42	6.62	-0.2
40		H	Meta	C	1.48	5.83	5.87	-0.04
41		H	Para	C	0.287	6.54	6.65	-0.11
42		H	Meta	C	2.58	5.59	5.69	-0.1
43		H	Para	C	0.154	6.81	5.98	0.83
44		H	Meta	C	0.657	6.18	5.83	0.35
45*		H	Para	C	0.124	6.91	6.69	0.22

* Used as an external test set

together with donepezil, totally 45 compounds are listed in Table 1. The AChE inhibition activity (IC_{50}) values for the dataset molecules vary from 0.03 to 22 μM (a factor of about 22,00), and were measured in vitro according the modified Ellman method using rat cortex homogenate (AChE) (Cheng and Tang, 1998; Ellman *et al.*, 1961). The structures and AChE inhibitory activity (IC_{50}) data of these 44 molecules are listed in Table 1. The IC_{50} values were in micromolar (μM) range therefore, converted to the molar (M) range and then to its logarithmic scale (pIC_{50} , M), to reduce the skewness of the dataset, which was then used for subsequent QSAR analysis (Eq. 1) as the response variable.

$$\text{pIC}_{50} = -\log \text{IC}_{50} \quad (1)$$

Ten compounds (compounds with asterisks in Table 1) were randomly selected as external test set for further model validation, and the rest of the 34 compounds served as a training set to build 2D QSAR models. The 3D structures of these compounds were sketched and converted to 3D using ChemOffice2004 (<http://www.cambridgesoft.com>). The energy minimization was performed using Austin Model-1 (AM1) (Dewar *et al.*, 1985) until the root mean square

(RMS) gradient value became smaller than 0.100 kcal/mol \AA and then molecules were subjected to re-optimization via MOPAC (Molecular Orbital Package) method until the RMS gradient attained a value lesser than 0.0001 kcal/mol \AA using MOPAC (<http://www.ccl.net>).

Generation of structure-based pharmacophore models and virtual screening

A set of five pharmacophore hypotheses were generated based on three available AChE inhibitor complexes taken from the PDB (PDBid: 1EVE, 1GQR and 1ACJ). Pharmacophore hypothesis generation was performed with the LigandScout 3.0 software (Wolber and Langer, 2005). Maybridge small molecule database was used to screen the compounds. The software extracts and interprets ligand–receptor interactions such as hydrogen bond, charge transfer, hydrophobic regions of their macromolecular environment from PDB files. Alternative hydrogen bond acceptor (HBA) and/or hydrogen bond donor (HBD) sites are considered simultaneously on the protein within the limits of geometric constraints. Excluded volume spheres were also added to the structure-based model onto

coordinates defined by protein side chain atoms to characterize the inaccessible areas for any potential ligand.

Molecular docking

The docking of the 44 1-indanone derivatives and hits ligands into the catalytic and peripheral binding site of AChE was performed using the AutoDock v.4.0 (Morris *et al.*, 2009). In order to compare the results from docking protocols, water molecules and other ligand (NAG) were excluded for the better docking score; the protonation state (donepezil, E20 and 1EVE) were set to the physiological pH since the protonation states of HIS 440 residue in AChE protein were chosen to get the sensible hydrogen bonding network where as ligand, E20 has a pKa value of 8.82 so at physiological pH it would coexist both, protonated and non-protonated forms. The rotatable bonds of the ligands were set to be free; and the protein was treated as a rigid body (Gupta *et al.*, 2011). Crystal structure of the AChE protein (1EVE) was retrieved from PDB databank (<http://www.pdb.org/>) (Berman *et al.*, 2000; Kryger *et al.*, 1999). Rigid docking was performed for studying protein–inhibitor interactions through AutoDock Tools. The atom types and bond types were assigned (Bikadi and Hazai, 2009; Labute, 2009). The polar hydrogen atoms of the enzymes were added, the non-polar hydrogen atoms were merged, Gasteiger charges were assigned, and solvation parameters were added. For all ligands, including E20, the non-polar hydrogen atoms were merged, and the Gasteiger charges were assigned. The auxiliary program AutoGrid generated the grid maps. The grids, one for each atom type in the ligands, plus one for the electrostatic interactions, were chosen so as to be sufficiently large to include the active site of AChE, since all ligands are bonded within the active site. The grid box dimensions were $60 \times 60 \times 60$ Å around the active site and the grid spacing was set to 0.375 Å. The starting positions of all ligands were outside the grid box (>20 Å away from the center of the binding pocket).

Docking was performed using the empirical free energy function together with the Lamarckian genetic algorithm (LGA) (Mashhadi *et al.*, 2003). The LGA protocol applied a population size of 150 individuals, while 250,000 energy evaluations were used for the 20 LGA runs. In addition, the maximum number of evaluations was set to 27,000; the mutation rate to 0.02; the crossover rate to 0.8; and the elitism rate to 1.0. Generated conformations had an associated value of binding free energy. Estimated inhibition constants (K_i) were used for determination of binding energies of different docking conformations, ranking in accordance to their binding scores (Morris *et al.*, 2009; Gupta *et al.*, 2012a, b). The calculated properties of K_i ,

binding free energy, electrostatic energy, van der Waals, hydrogen bond, desolvation energy, total intermolecular, and torsional energy for 44 1-indanone derivatives and 14 screened hits given in Tables 2 and 3, respectively. Chimera and Discovery Studio (DS) Visualizer2.5 (Pettersen *et al.*, 2004) software were used for visualization and calculation of protein–ligand interactions.

Descriptor calculation and selection

The descriptors were calculated using the web-based PreADMET tool (Lee *et al.*, 2003), ACD/ChemSketch software (<http://www.acdlabs.com>), and Chemoinformatics package of Chemaxon (<http://www.chemaxon.com>) which includes: electronic descriptors, topological descriptors, geometrical descriptors, structural descriptors, physico-chemical descriptors, thermodynamics descriptors, and ADMET descriptors. Before starting with the development of the QSAR model, the correlation matrix of about 1,100 descriptors was calculated and highly correlated descriptors, with correlation values above 0.7, were removed. Auto scaling method was adopted to avoid any bias due to strongly diverging descriptor values (Friedman and Roosen, 1995). Furthermore, descriptors with constant values as well as those with poor correlation to the biological property were discarded; some descriptors having zero value were also discarded. Finally, four class of descriptors: thermodynamic (TD), electronic (ED), geometrical (GD), and physicochemical (PD), were considered for statistical fitting using multiple linear regression (MLR).

Multiple linear regression analysis (MLR)

MLR analyses were performed by using XLSTAT software (www.xlstat.com) for the four classes of descriptors (TD, ED, GD, and PD) as independent variables while the pIC_{50} values were used as dependent variables. In the statistical analysis, a systematic search was performed to determine the significant descriptors. In order to minimize the effect of collinearity and to avoid redundancy, correlation matrices were developed and the variables which showed exact linear dependencies between subsets of the variables and multiple collinearity (high multiple correlations between subsets of the variables) were removed from the analysis. In order to explore the reliability of the proposed model, we used the cross-validation method. Prediction error sum of squares (PRESS) is a standard index to measure the accuracy of a modeling method based on the cross-validation technique. The q^2 calculated using Eq. (2) based on the PRESS and the sum of squares of the deviations of the experimental values from their mean (SSY).

Table 2 E20/1EVE complex and 44 1-indanone derivatives corresponding energies and RMSD (Å) difference values obtained from the re-docking validation/docking test performed using AutoDock program

Compound no.	E^b (kcal/mol)	$V_{dw}-H_b-D_s$ (kcal/mol)	I^c (kcal/mol)	BE^e (kcal/mol)	K_i (nM)	RMSD (Å)
E20	-0.96	-10.09	-0.55	-9.95	50.55	1.934
2	-0.96	-8.44	-0.41	-8.16	1004.00	91.839
3	-1.02	-8.64	-0.72	-8.73	399.71	92.738
4	-1.11	-9.01	-0.63	-9.11	208.77	91.749
5	-0.98	-9.04	-0.17	-8.55	543.47	91.045
6	-0.78	-8.40	-0.93	-7.91	1590.00	90.202
7	-0.80	-8.83	-0.84	-8.27	865.03	92.915
8	-0.76	-8.69	-0.76	-8.01	1340.00	91.581
9	-0.96	-8.46	-0.79	-8.02	1330.00	91.459
10	-0.89	-9.38	+0.03	-8.59	505.09	92.580
11	-0.89	-9.39	-0.73	-9.36	137.63	92.673
12	-0.86	-9.05	-0.73	-8.99	257.10	92.904
13	-0.82	-8.73	-0.82	-8.72	402.85	92.466
14	-0.99	-8.87	-0.75	-8.97	266.41	92.661
15	-0.84	-10.04	-0.89	-10.12	38.18	92.737
16	-0.86	-8.70	-0.81	-8.72	403.05	92.301
17	-0.70	-9.55	-0.91	-9.51	106.26	92.724
18	-0.74	-8.57	-0.66	-8.32	793.14	92.628
19	-0.90	-9.66	-0.54	-9.45	118.04	93.038
20	-0.73	-9.16	-0.34	-8.58	514.05	92.097
21	-0.41	-9.89	-0.44	-9.09	217.13	92.320
22	-2.25	-8.46	-0.77	-9.83	62.06	91.049
23	-2.04	-9.20	-0.10	-9.70	77.66	91.822
24	-2.44	-8.37	-0.60	-9.77	69.46	92.023
25	-1.97	-7.97	-0.77	-9.06	227.94	92.530
26	-1.31	-9.30	-0.59	-9.83	62.25	91.536
27	-0.82	-8.51	-0.52	-8.47	616.70	91.474
28	-1.20	-8.90	-0.58	-9.04	235.50	91.626
29	-1.14	-8.37	-0.37	-8.24	919.62	91.673
30	-0.96	-9.27	-0.73	-9.04	236.52	92.240
31	-0.80	-9.31	-0.47	-8.65	453.15	91.272
32	-0.98	-9.16	-0.64	-9.41	126.75	92.027
33	-0.74	-9.74	-0.04	-9.14	198.49	91.866
34	-1.00	-9.53	-0.60	-9.75	70.90	92.551
35	-1.19	-9.51	-0.25	-9.58	95.21	92.403
36	-0.77	-8.99	-0.45	-8.57	524.99	92.145
37	-1.17	-9.14	-0.60	-9.27	161.03	91.662
38	-0.85	-8.98	-0.68	-8.59	506.78	92.885
39	-0.61	-9.20	-0.34	-8.24	918.25	92.109
40	-1.11	-10.74	-0.80	-10.46	21.66	91.701
41	-1.03	-8.55	-0.78	-8.16	1040.00	90.244
42	-1.19	-10.44	-0.46	-10.44	22.28	91.492
43	-0.96	-8.36	-0.66	-8.34	772.65	91.830
44	-0.80	-10.12	-0.58	-9.86	59.34	92.296
45	-0.87	-9.73	-0.78	-9.73	73.78	91.890

E^b The electrostatic component of binding free energy in kcal mol⁻¹, $V_{dw}-H_b-D_s$ Van der waals, hydrogen bond-desolvation energy component of binding free energy in kcal mol⁻¹, I^c Total internal energy of binding in kcal mol⁻¹, BE^e Estimated binding free energy in kcal mol⁻¹, K_i Inhibitory constant in nanomolar, $RMSD$ Root mean square deviation

Table 3 Screened 14 hits from Maybridge database, corresponding energies and RMSD (Å) difference values obtained from the re-docking validation test performed using AutoDock program

Maybridge comp.	E^b * (kcal/mol)	$V_{dw}-H_b-D_s^*$ (kcal/mol)	I^c * (kcal/mol)	BE^{c*} (kcal/mol)	K_i^* (nM)	RMSD* (Å)
AW00841	-0.68	-9.47	-1.03	-8.98	263.15	90.357
BTB15236	-0.81	-11.85	1.18	-9.84	61.40	91.479
GK02443	0.49	-10.49	-0.23	-7.75	2,070	90.918
GK02444	0.05	-10.74	-0.35	-8.57	521.34	89.491
GK02445	0.51	-10.36	-0.03	-7.68	2,350	90.466
HTS01811	-0.86	-8.62	-0.1	-9.03	241.14	92.321
HTS02407	-1.27	-9.05	-0.41	-9.91	54.84	90.473
HTS03170	-0.63	-11.33	-0.16	-10.47	21.29	93.559
HTS06574	-2.33	-8.49	-0.54	-9.99	47.34	92.192
HTS09726	-0.79	-9.33	-0.56	-9.58	95.30	91.637
KM08871	-0.98	-10.01	-0.8	-10.43	22.78	92.983
S03906	-0.17	-10.19	-0.96	-9.39	130.05	90.122
S15017	-0.19	-9.31	-0.12	-8.25	896.73	90.434
SEW05768	0.14	-8.42	-0.66	-7.56	2,870	91.076

* Abbreviations as in Table 2

$$q^2 = 1 - \frac{\text{PRESS}}{\text{SSY}} = 1 - \frac{\sum_{i=1}^n (y_{\text{exp}} - y_{\text{pred}})^2}{\sum_{i=1}^n (y_{\text{exp}} - \bar{y})^2} \quad (2)$$

QSAR model validation

The QSAR model developed was evaluated rigorously using *Y* randomisation test (Rucker *et al.*, 2007) and test set predictions. *Y* randomisation test confirms whether the model is obtained by chance correlation, and is a true structure–activity relationship to validate the adequacy of the training set molecules. The steps followed in the randomisation test are (1) repeatedly the activity data were scrambled in the training set molecules, (2) the randomised data was used to generate QSAR equations, and (3) the resulting scores were compared with the score of the original QSAR equation generated with non-randomised data set. If the activity prediction of the random model was comparable to that of the original equation, the set of observations was not sufficient to support the model. The randomisation test was performed at different confidence intervals (90, 95, and 99 %). More randomisation tests are run for higher confidence levels. For a 90 % confidence level, there were 7 trials run, 17 trials for 95 %, and 97 trials for 99 %. The correlation coefficient (*r*) value of the original model was much higher than any of the trials using permuted data, hence showing that the model developed was statistically significant and robust. The predictive properties of the developed QSAR model were tested more rigorously by predicting the AChE inhibitory potency of ten test set molecules.

Result and discussion

The general strategy for the ligand and structure-based virtual screening pursued in the present study is presented in Fig. 1. The pharmacophore hypothesis generated first using PDBid 1EVE, 1GQR, and 1ACJ. To validate the pharmacophore, docking of 44 1-indanone derivatives was performed, and the docking pose was overlapped in the generated pharmacophoric features. Maybridge small database were subjected to 3D pharmacophore search. The virtually screened hits (new scaffold) were then prioritized by matching the docking pose with pharmacophore, and QSAR analysis was done to predict the activity of virtually screened hits.

Generation and validation of structure-based pharmacophore models using LigandScout

LigandScout extracts and interprets the interactions between protein and ligand as well as with some excluded volume spheres corresponding to the 3D structure of protein. In this study, three different 3D structure of AChE bound with its known inhibitors such as 1EVE, 1GQR, and 1ACJ were selected as input for structure-based pharmacophore generation. The inhibitors used for pharmacophore generation are listed in Fig. 2 and five pharmacophore hypothesis generated from the PDB complex ligands are presented in Fig. 3. For 1EVE complex, (Hypo I), the generated pharmacophore contains one hydrophobic pointed toward ILE444, TRP84, three HBA, two HBD, one positive ionizable (PI) toward TRP84, PHE330, and 11

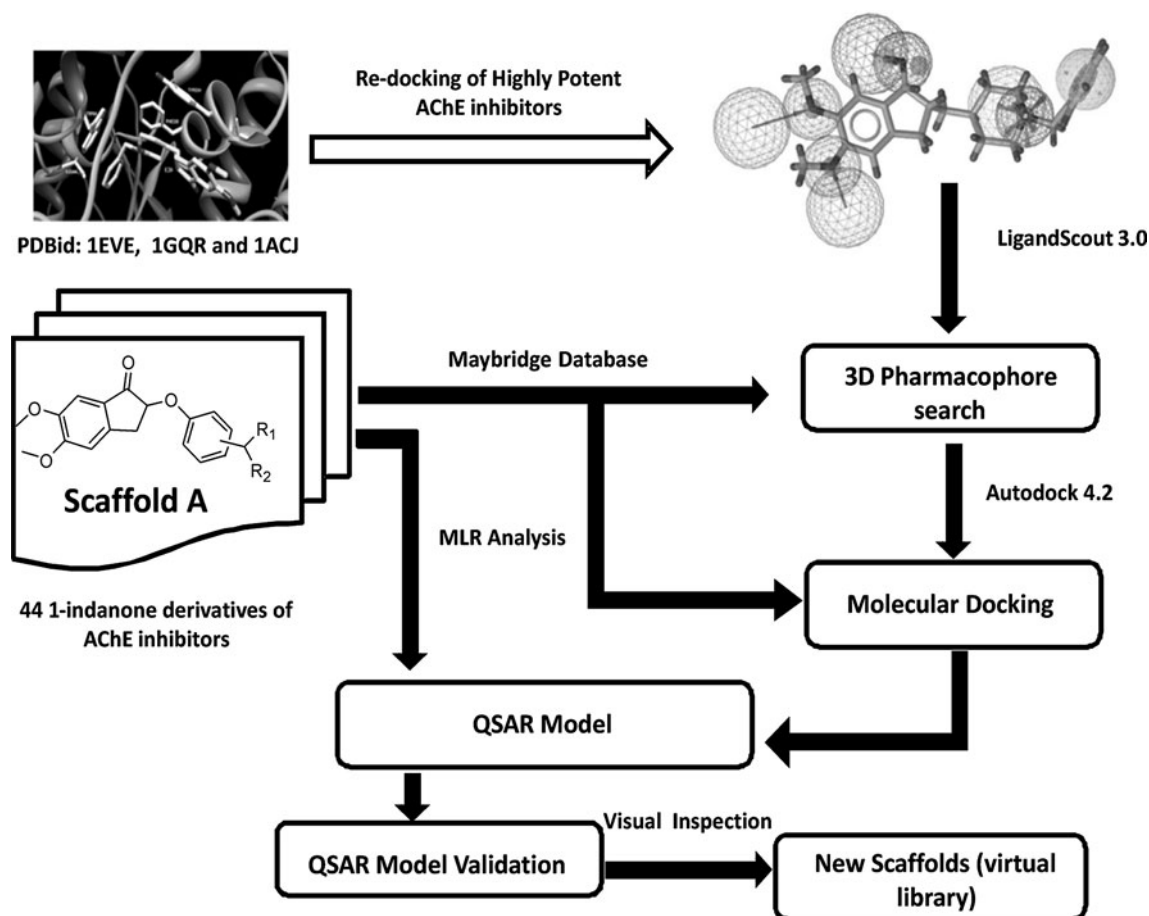


Fig. 1 Scheme of the structure-based virtual screening protocol for identification of Alzheimer AChE inhibitors targeted virtual library. Initially, the generation of pharmacophore hypothesis was done using PDBid 1EVE, 1GQR, and 1ACJ. In the next step, Maybridge database of 60,538 molecules were subjected to 3D pharmacophore search and

then to high throughput docking. In the final step, 44 1-indanone derivatives were used for generation of QSAR equation and selection of new potent scaffold was done based on scoring quantitative structure activity relationship model

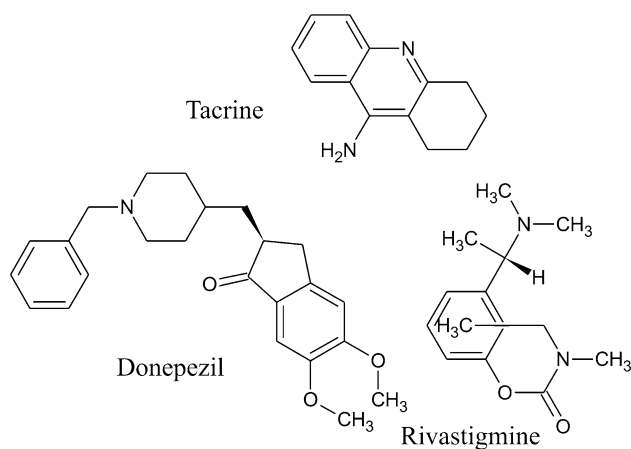


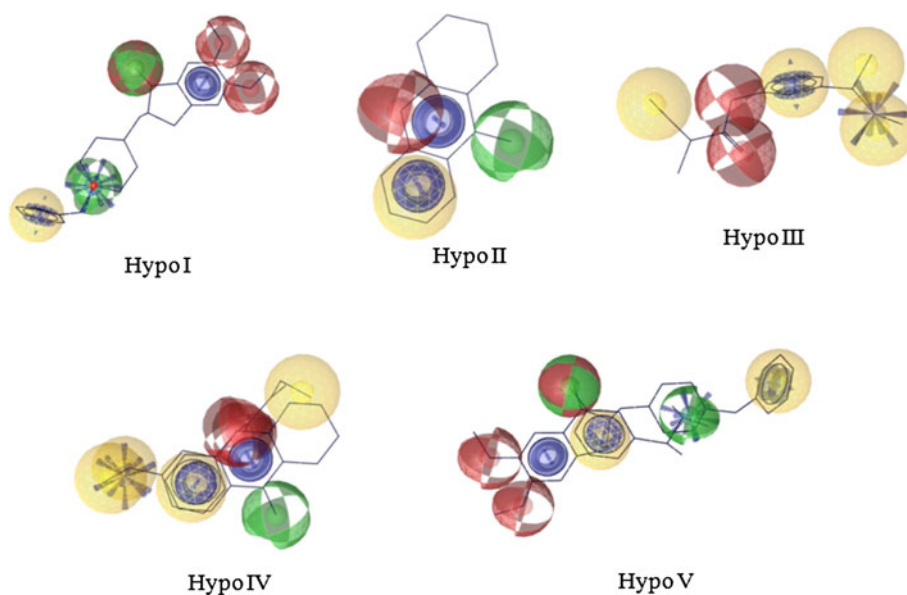
Fig. 2 AChE inhibitors selected for pharmacophore hypothesis generation

excluded volume sphere. Three features hypothesis was generated from 1ACJ complex, (Hypo II), which composed of one hydrophobic toward ILE444, TRP84, two HBD, and

nine excluded volume sphere. 1GQR complexes, (Hypo III), consist of seven features hypothesis includes four hydrophobic toward TRP84, PHE330, two HBA toward ALA201, GLY118, GLY119, one PI pointed toward GLU199, TRP233, and 13 excluded volume sphere. The dynamic structure-based pharmacophore was generated by superimposing the 1ACJ & 1GQR, (Hypo III); 1EVE & 1GQR, (Hypo IV), and the overlapped chemical features were removed. Finally, eight features structure-based hypothesis (Hypo V), was produced that consists of four hydrophobic, two HBA, one HBD, one PI, and 18 excluded volume sphere and two hydrophobic, three HBA, two HBD, one PI, and 19 excluded volume sphere, respectively.

The validity of any pharmacophore model needs to be determined by applying that model to the test set to find out how correctly the model predicts the activity of the test set molecules and, most importantly, whether it can identify active and inactive molecules correctly or not. The pharmacophores were validated by accessing the predictive ability of the pharmacophore on test set database consisting

Fig. 3 Five pharmacophore hypotheses generated using three AChE inhibitors (Color figure online)



of 44 known inhibitors of AChE (Sheng *et al.*, 2005) and a subset of World of Molecular Bioactivity (WOMBAT) database consisting of 502 molecules, active against different proteins other than used in present study, considered here as inactive. This validation gives confidence to select the best pharmacophore among the five pharmacophores generated. The results for pharmacophore validation are summarized in Table 4. A number of parameters such as hit list (H_t), number of active percent of yields (% Y), percent ratio of actives in the hit list (% A), enrichment factor (E), false negatives, false positives, and goodness of hit score (GH) (Table 4) (Wolber and Langer, 2005). The pharmacophore hypothesis (Hypo I in Table 4; Fig. 4) with minimal false positives and negatives, good enrichment factor, and goodness of fit score was considered as best model for virtual screening among the five pharmacophore hypotheses. In 44 molecules predicted to be active, 43 molecules were correctly picked, thus missing only one

false negative with only eight false positive. In pharmacophore hypothesis 3, (Hypo III) six false positives were found, but only 12 actives were picked among the 44 actives. In addition, hypo I and hypo III have shown an enrichment factor of 10.463 and 8.273 as well as the GH score of 0.863 and 0.561, respectively, which indicates that the quality of the pharmacophore models are acceptable. By overall validations, it was sure that the hypo I was good enough to discriminate the active inhibitors from inactive or low active compounds.

Virtual screening

From the above validation methods, it was proved that hypo I have superior ability to distinguish the active and inactive inhibitors of AChE. The representative pharmacophore hypo I (Fig. 4), have used as a 3D queries to screen the chemical database, Maybridge which consists of

Table 4 Statistical parameters from screening AChE test set molecules

No.	Parameter	Hypo I	Hypo II	Hypo III	Hypo IV	Hypo V
1	Total number of molecules in the database (D)	546	546	546	546	546
2	Total number of actives in the database (A)	44	44	44	44	44
3	Total hits (H_t)	51	85	18	122	197
4	Active hits (H_a)	43	4	12	28	37
5	% yield of actives ($H_a/H_t \times 100$)	84.314	4.705	66.667	22.951	18.782
6	% ratio of actives ($H_a/A \times 100$)	97.727	9.091	27.273	63.636	84.091
7	Enrichment factor (E) ^a	10.463	0.584	8.273	2.848	2.331
8	False negatives ($A - H_a$)	1	40	32	16	7
9	False positives ($H_t - H_a$)	8	81	6	94	160
10	Goodness of hit score (GH) ^b	0.863	0.049	0.561	0.269	0.2392

^a $E = H_a D / H_t A$

^b $GH = (H_a / 4H_t A) (3A + H_t) \times (1 - [(H_t - H_a) / (D - A)])$

Fig. 4 Seven features hypothesis: hypo I and its geometric constraints. *Yellow* color indicates hydrophobic (H); *green* color indicates HBD; *red* color indicates HBA; and *blue* color indicates positive ionizable (PI) (Color figure online)

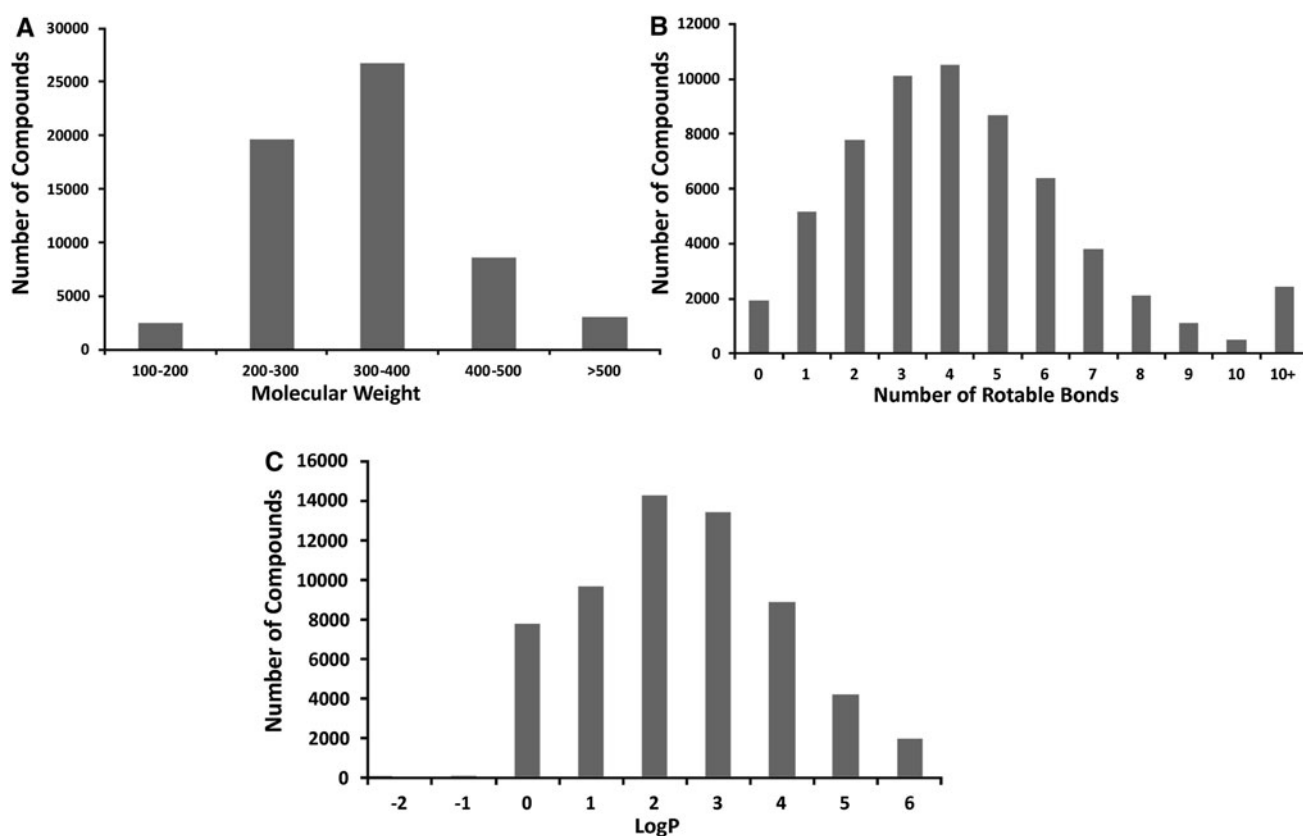
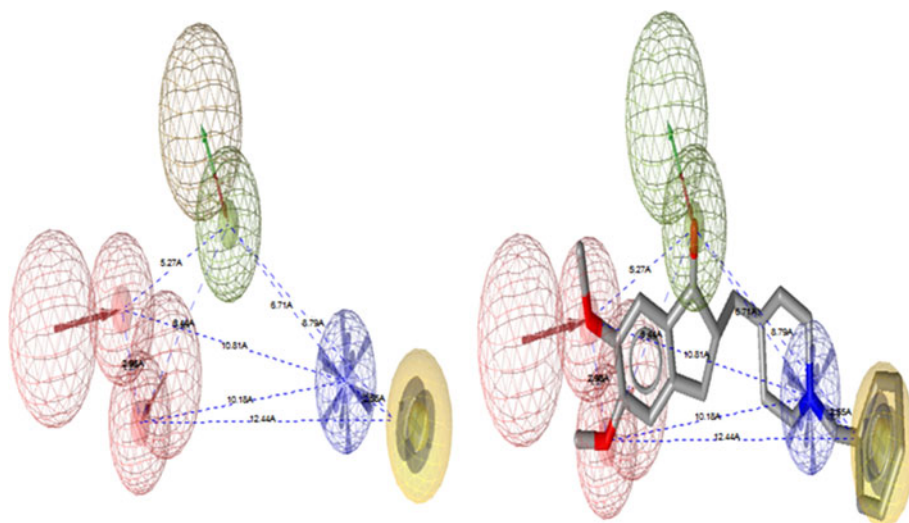


Fig. 5 Physicochemical profile of the Maybridge 60,538-compound collection: **a** molecular weight; **b** number of rotatable bonds; and **c** log *P*

60,538 compounds. We focused on three properties/descriptors, molecular weight, number of rotatable bonds and log *P* values (Lipinski *et al.*, 2001; Veber *et al.*, 2002; Walters and Murcko, 1998). As seen in Fig. 5, Maybridge collection has values for these three properties consistent with drug-like rules. For ~95 % of the compounds, the MW is between 100 and 500 Da, with ~32 % of the compounds having a MW between 200 and 300 Da

(Fig. 5a). Concerning the number of rotatable bonds, 93 % of the compounds have between zero (rigid) and eight flexible bonds, with 58 % of the compounds having less than five rotatable bonds (Fig. 5b). The calculated log *P* values range from -2 (more polar) to 5 (more hydrophobic) for 96 % of the compounds (Fig. 5c). Thus, we believe that this Maybridge collection is sufficiently diverse in term of MW, log *P* and number of rotatable

Table 5 ADME values for the selected compounds from Maybridge database which satisfied all the chemical features of Hypo I

Maybridge comp.	Blood brain barrier BBB (C.brain/C.blood)	Skin permeability (log Kp)	Human intestinal absorption (HIA %)	Plasma protein binding (%)
AW00841	0.206	−3.394	98.49	82.93
BTB15236	0.262	−2.251	98.82	92.49
GK02443	0.431	−1.664	92.08	100
GK02444	0.491	−1.73	94.53	99.59
GK02445	0.311	−1.97	95.22	100
HTS03170	0.424	−2.27	96.97	95.54
HTS01811	4.794	−1.78	96.02	84.97
HTS06574	3.417	−2.06	96.74	99.86
HTS09726	0.103	−3.75	95.94	68.77
HTS02407	0.282	−3.72	96.31	78.53
KM08871	6.132	−1.64	96.49	91.75
S03906	0.033	−3.44	95.68	94.7
S15017	4.232	−1.83	95.14	90.34
SEW05768	0.211	−1.77	97.91	100

Table 6 Equation of quantitative structure–activity relationship (QSAR) models with increasing number of descriptors

Number of descriptors/QSAR model	r^2	QSAR equation
3 (Model 1)	0.541	$\text{pIC}_{50} = 4.72889 + 9.24710^{**}\text{HBA} + 5.42041^{**}\log P + 1.18031^{**}\text{HOF}$
4 (Model 2)	0.562	$\text{pIC}_{50} = 1.94019 + 1.36462^{**}\text{HBA} + 1.48636^{**}\log P + 1.51832^{**}\text{HOF} + 1.65393^{**}\text{EE}$
5 (Model 3)	0.723	$\text{pIC}_{50} = 5.47636 + 9.48144^{**}\text{HBA} + 9.94758^{**}\log P + 1.54583^{**}\text{HOF} + 1.24818^{**}\text{EE} - 1.71727^{**}\text{DIPOLE}$
6 (Model 4)	0.703	$\text{pIC}_{50} = 4.55119 + 9.33649^{**}\text{HBA} + 1.05744^{**}\log P + 1.33585^{**}\text{HOF} + 1.23332^{**}\text{EE} - 1.62974^{**}\text{DIPOLE} - 4.54135^{**}\text{LUMO}$
7 (Model 5)	0.670	$\text{pIC}_{50} = 4.41032 + 9.25509^{**}\text{HBA} + 1.03818^{**}\log P + 1.29898^{**}\text{HOF} + 1.29336^{**}\text{EE} - 1.62256^{**}\text{DIPOLE} - 4.67832^{**}\text{LUMO} + 5.79261^{**}\text{PAR}$

HBA hydrogen bond acceptor, *log P* solubility, *HOF* heat of formation in kcal, *DIPOLE* dipole moment in Debye, *EE* electronic energy in electron volt, *LUMO* lomo energy in electron volt, *PAR* parachlor in cm^3

bond and suitable for a virtual screening study. Overall, the active compounds display similar properties as the other molecules present in Maybridge database. The Maybridge small molecule database consisting of 60,538 molecules were translated into a LigandScout database using the database generation (idbgen) function of LigandScout 3.0. In total only 14 compounds were screened from Maybridge database which satisfied all chemical features present in hypo I. These 14 hits were used for further analysis like molecular docking studies to avoid false-positive hits from the screening process. The final leads of hypo I were also calculated for ADME and Drug likeness properties as tabulated in Table 5.

Docking using Autodockv 4.0

Molecular docking provides a visualization of potential binding orientations that display clearly the hydrogen bonding interaction with critical residues such as TRP84

and PHE330. The 44 1-indanone derivatives and 14 new screened hits were docked to AChE protein using LGA. The docking results, the predicted binding energies, inhibitory constant, and interactions have been calculated for all of them (Tables 2, 3; Fig. 6). GLY118, TYR121, SER122, GLY123, TYR130, SER200, PHE288, and PHE331 residues comprising of catalytic binding site where as the peripheral binding site consists of residues TRP84, TRP279, PHE330, and TYR334 (Fig. 7).

An example of scaffold B, 2-substituted 1-indanone inhibitor compound no. **33** (Table 1), the potent inhibitor with minimum binding energy was selected to illustrate the detailed interactions between inhibitors and the enzyme. As discussed later, the descriptions referred to compound no. **33**, unless otherwise specified. Figure 8 shows the binding mode of compound no. **33** with AChE. In general, these inhibitors could be divided into three parts: the 5,6-dimethoxy-1-indanone moiety, the benzene ring moiety, and the protonated nitrogen moiety (Sugimoto *et al.*, 2000).

Fig. 6 44 1-Indanone derivatives and 14 Maybridge hits interactions with the key residues involved in AChE activity

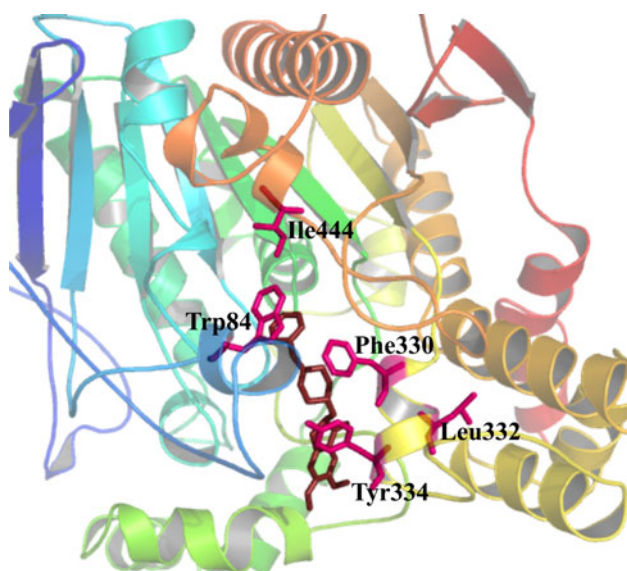
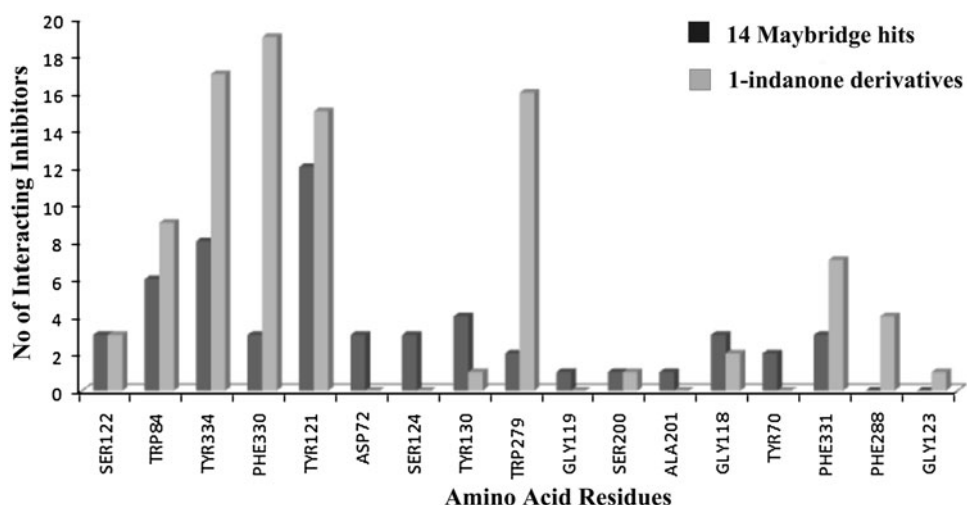


Fig. 7 Cartoon representation of the whole protein with localization of known binding pockets TRP84, GLY123, PHE288, PHE330, PHE331, and TYR334 are some of the residues (Color figure online)

All the inhibitors formed major interactions with the catalytic and peripheral binding site of the enzyme through the three parts (Kaur and Zhang, 2000).

The 5,6-dimethoxy-1-indanone moiety of all the compounds was approximately located at the same site. It was obvious to see that the 5,6-dimethoxy-indanone moiety was surrounded by hydrophobic residues TRP84, TYR121, PHE290, and PHE330 (Fig. 8). Among scaffold A, B, and C (Table 1), the indanone group formed a π - π stacking interaction with the indole ring of TRP84, TRP279, TYR334, and PHE33, while the 5,6-dimethoxy group of scaffold A and C interacted with the side chains of TYR121 through the hydrogen bonding. The carbonyl group of the 5,6-dimethoxy-1-indanone moiety of scaffolds

A and C, as an acceptor formed a hydrogen bond with the NH group of GLY118, GLY123, PHE288, and PHE331.

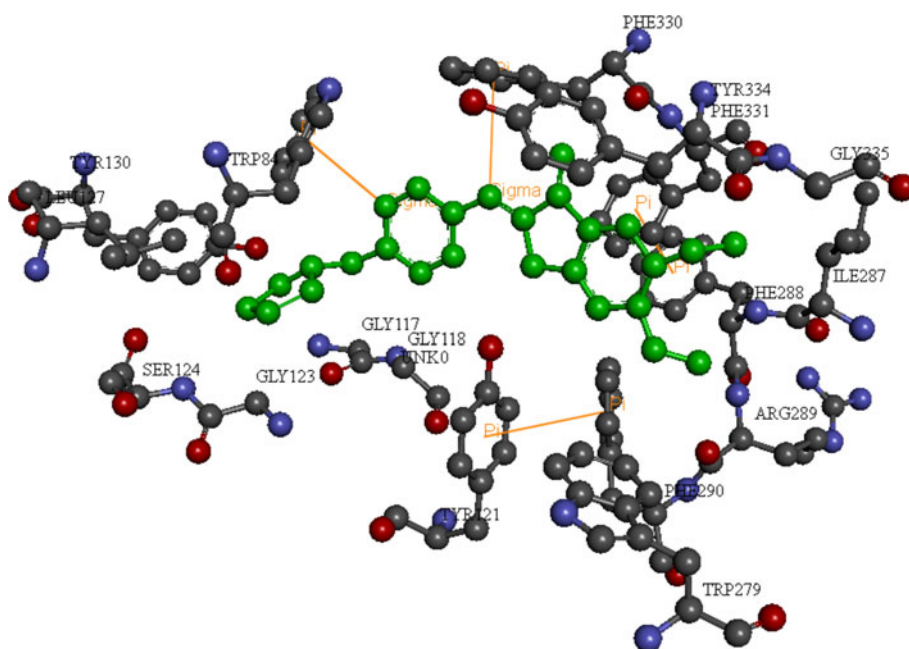
The new scaffolds obtained from virtual screening hits showed π - π stacking interaction and hydrogen bonding within the binding pocket of AChE. The promising compounds share common pharmacophoric features like a nitrogen-rich scaffold (pyridine, pyrazole, piperidin, amides, piperazine, etc.). The predicted binding modes of Maybridge hit HTS02407 and HTS03170, kept in scaffold H, are shown in Fig. 9. Like most of the AChE inhibitors, identified hits are all anchored to the cavity by hydrogen bonds between the ligand and TYR121 (catalytic binding site) and π - π stacking interaction with TRP84 and PHE330 (peripheral binding site). Aromatic rings of compounds HTS02407 (Fig. 9a) and HTS03170 (Fig. 9b) are embedded in the subpocket formed by GLY118 and TYR121 residues. These compounds interact via hydrogen bonding.

Descriptor calculation, selection, and multiple linear regression analysis (MLR)

A QSAR analysis was performed to explore the structure-activity relationship of different scaffolds of 1-indanone derivatives as AChE inhibitors. These 2 substituted 1-indanone inhibitors possess a variety of scaffolds (A, B and C) with different protonated nitrogen moiety as presented in Table 1. The dataset of 44 molecules was divided into a training set of 34 molecules and a test set of 10 molecules taking into account structural diversity and activity range. The training set molecules were then used to generate the QSAR models, while the test set molecules were selected for model validation.

The 2 substituted 1-indanone type dataset has three different structurally diverse scaffolds, as given in Table 1. Scaffold A has 24 molecules (2–25), with activity ranging from 0.05 to 22.1 μ M. Scaffold B has 10 molecules (26–35),

Fig. 8 Interaction of compound no. 33 with AChE. Inhibitor and the key residues within 4.0 Å around the inhibitor in AChE are represented by the ball-and-stick and stick models, respectively. Orange lines denote the hydrogen bond. This image was generated with the Discovery Studio Program (Color figure online)



with activity ranging from 0.035 to 2.14 μM . Other series of molecules from the dataset include scaffold C, with 10 molecules (36–45), and activity ranging from 0.124 to 3.74 μM . Table 1 shows the structure and activity of these three different scaffold-containing molecules. The most potent molecules (31 and 33) are present in the scaffold C group. The contribution of the electronic environment of the descriptor (EE) in these two molecules has similar chemical features, as reflected in its R1 and R2 substitutions at para position. The presence of this descriptor is very important for the potent activity of these molecules, which was further confirmed by the positive slope in QSAR model 3 (Table 6). Further, the functional groups attached at the R1 region in molecules 31 and 33 have aromatic features.

The scaffold A has the least potent molecule (19) with an IC_{50} value of 22.1 μM , which is 1,000-fold less potent than molecule 31. The R1-morpholine group substitution at meta position in molecule 19 favoring lower activity (Table 1). The presence of an HBA descriptor of lower slope type chemical feature might be the key point determining the low activity of molecule 19. We also analyzed the contribution of different descriptor values in QSAR model 3 for log P and heat of formation (HOF) descriptors, with respect to the most potent molecules 31 and 33 as well as that of the least potent molecule 19. These values were used mainly for the development of QSAR model 3. For the most potent molecules 31 and 33, the log P descriptor has a descriptor value of 4.23. For the least potent molecule 19, this value is 2.71. The positive correlation of the log P descriptor in building QSAR model 3 revealed that, for the most potent molecules, its contribution (or descriptor value) should be more, and for the least potent molecules its contribution

should be less. Thus, the low descriptor value of the log P descriptor for molecule 19 suggests its contribution in making the molecule less active. On the other hand, the most potent molecules (31 and 33) have higher descriptor values as mentioned above, suggesting that the contribution of log P descriptor was more, which in turn favor greater molecular activity. The HOF descriptor has descriptor values -65.58 and -61.82 for the most potent molecules 31 and 33. For the least potent molecule 19, this value was -151.81 , which was more than that observed for the log P descriptor as mentioned above. This analysis shows clearly that the positive contribution of the value of the descriptors log P and HOF in generating QSAR model 3 was in agreement with each molecule's AChE activity. Thus, the above analysis clearly demonstrated that the influence of log P and HOF descriptors was very important in distinguishing between potent and less potent 1-indanone AChE inhibitors. Based on the findings derived from the developed MLR model, the biological activity of 14 selected hits was predicted, shown in Table 7. As expected, the predicted activity more than 3/4th of the virtual screening hits, i.e., 85.71 % was higher than the reported experimental activity of donepezil AChE inhibitor ($-\log\text{IC}_{50}$ of 7.80 for 2 substituted derivative of 1-indanone, (compound 1 in Table 1).

Sensitivity of the QSAR model

Sensitivity of the QSAR models was assessed mainly using two statistical parameters: the cross-validated correlation coefficient (q^2), and Fischer ratio (F). The correlation coefficient (r^2) can be increased easily by the number of

Table 7 Chemical structures of putative AChE binders and their respective docking scores, predicted activity, molecular weight and log *P* identified using virtual screening and QSAR

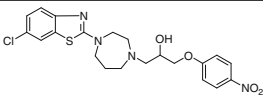
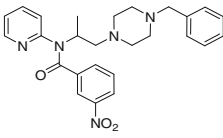
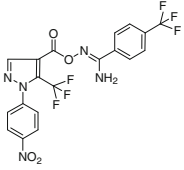
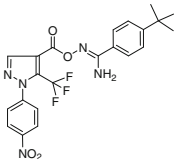
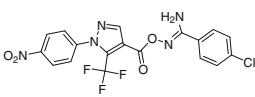
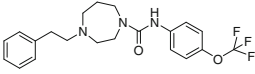
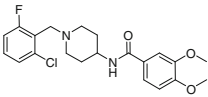
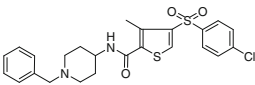
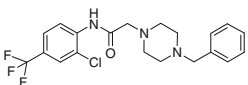
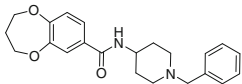
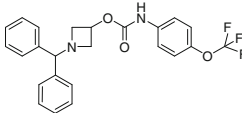
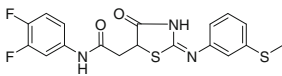
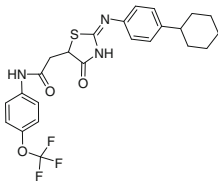
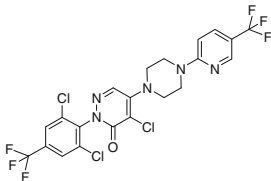
S.No	Maybridge ID	Structure	Docking Score	New Scaffold	Mol. Weight	LogP	pIC ₅₀
1.	AW00841		-8.98	E	462.95	4.37	11.94
2.	BTB15236		-9.84	F	459.54	4.25	13.06
3.	GK02443		-7.75	G	487.31	4.79	8.99
4.	GK02444		-8.57	G	475.42	5.46	11.4
5.	GK02445		-7.68	G	453.76	4.52	11.36
6.	HTS01811		-9.03	H	407.43	4.66	14.57
7.	HTS02407		-9.58	H	406.88	3.23	16.58
8.	HTS03170		-10.47	H	489.05	4.76	9.97
9.	HTS06574		-9.99	H	411.85	3.51	6.47

Table 7 continued

S.No	Maybridge ID	Structure	Docking Score	New Scaffold	Mol. Weight	LogP	pIC ₅₀
10.	HTS09726		-9.58	H	366.45	2.37	4.38
11.	KM08871		-10.43	I	442.43	6.66	12.49
12.	S03906		-9.39	J	407.46	4.06	8.28
13.	S15017		-8.25	J	491.53	6.69	6.55
14.	SEW05768		-7.56	K	572.72	6	7.63

terms in the QSAR equation, so we took q^2 as the limiting factor for controlling the number of descriptors to be used in the model. In order to assess the sensitivity, five different QSAR models were created by increasing the number of descriptors stepwise from three to seven. The QSAR equations along with the number of descriptors are presented in Table 6. Different statistical parameters used to validate these QSAR models are shown in Tables S1 in the electronic supplementary material (ESM). The variation of r^2 and q^2 values with the number of descriptors is presented in ESM Fig. S1. The r^2 and q^2 values increase until the number of descriptors in the QSAR equation reached five. When the number of descriptors in the QSAR equation was six (model 4), there was a decrease in q^2 value indicating the model sensitivity, as presented in Fig. S1 and Table S1. Thus, the number of descriptors was restricted to five and the QSAR equation (Eq. 3) obtained for model 3 is given below.

$$\begin{aligned} \text{pIC}_{50} = & 5.47636 + 9.48144 * \text{“HBA”} + 9.94758 \\ & * \text{“log } P\text{”} + 1.54583 * \text{“HOF”} + 1.24818 \\ & * \text{“EE”} - 1.71727 * \text{“DIPOLE”} \end{aligned} \quad (3)$$

$$\begin{aligned} N = 34; r^2 = 0.723, r_{\text{adj}}^2 = 0.971; F\text{-test} \\ = 13.298; \text{MSE} = 0.181; r = 0.898; q^2 = 0.703 \end{aligned}$$

where N is the number of molecules in the training set, r^2 is the squared correlation coefficient, r_{adj}^2 is the square of adjusted correlation coefficient, F -test is a variance-related statistic that compares two models differing by one or more variables to see if the more complex model is more reliable than the less complex one. The model is assumed to be good if the F test is above a threshold value, MSE is mean squared error, r is correlation coefficient, and q^2 is the square of the correlation coefficient of the cross-validation. Figure 10 presents a scatter plot of observed pIC₅₀ values for the training set (blue squares) and test set molecules

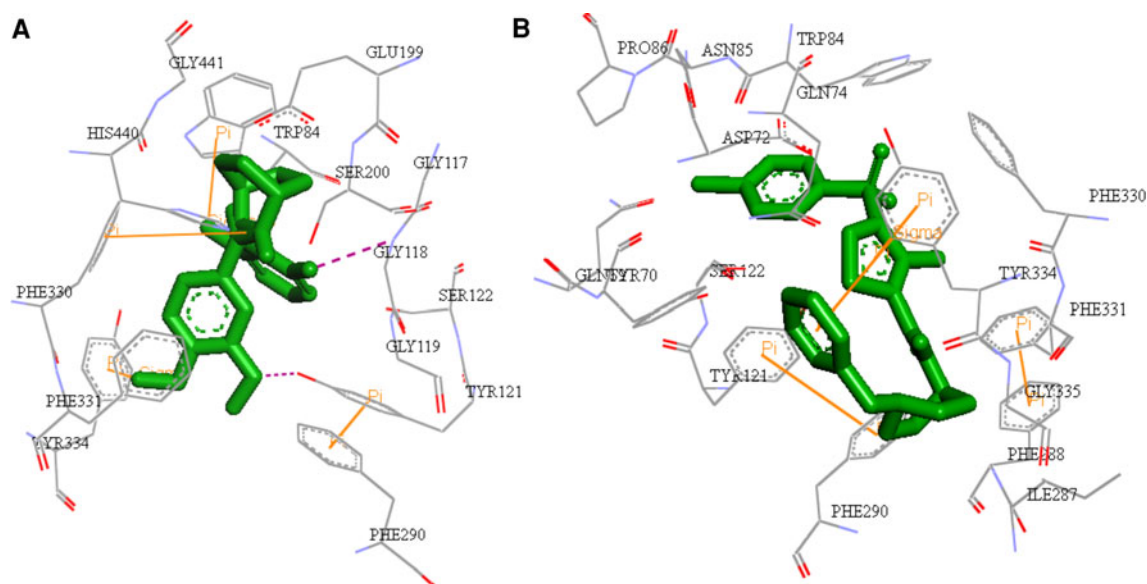


Fig. 9 Binding mode of Maybridge potential hits: **a** HTS02407; **b** HTS03170 (Color figure online)

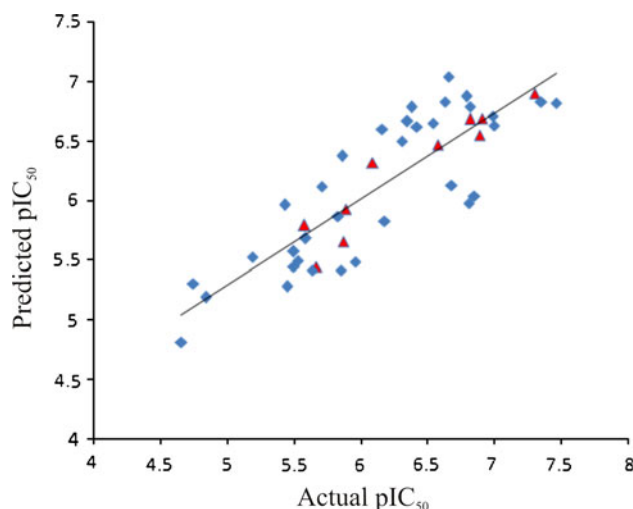


Fig. 10 Scatter plot of actual versus predicted activity of the training set (blue squares) and test set (red squares) molecules of QSAR model 3 (Color figure online)

(red squares) versus the calculated pIC_{50} values predicted by QSAR model 3.

Validation of the QSAR model 3

Cross-validation of the QSAR model 3 by the leave-one-out (LOO) procedure showed a statistically significant correlation coefficient of $q^2 = 0.703$. Furthermore, the randomisation test, performed for 97 random trials (Table S2) showed a large difference of about 0.6 in the r values for non-random and random trials, with the observed deviation of random values being 0.64, suggesting that the selected training set was adequate to support the developed

QSAR model. Also, none of the random r values were greater than the non-random r values. Furthermore, the correlation matrix of the descriptors used in developing the QSAR equation of model 3 is significant (presented in Table S3).

Conclusions

The work presented in this study shows that a set of compounds along with their activities ranging over several orders can be used to generate a good pharmacophore model, which in turn can be utilized to successfully predict the activity of a wide variety of chemical scaffolds. This model can then be used as a 3D query in database searches to determine compounds with various structures that can be effective as potent inhibitors and to assess how well newly designed compounds map onto the pharmacophore prior to undertaking any further research including synthesis. Biological evaluation and optimization in designing or identifying compounds as potential inhibitors of AChE were made possible by our pharmacophore study that showed the best model (Hypo I) of AChE inhibitors were made up of seven chemical features which was split into one hydrophobic, three HBA, two HBD, and one PI one hydrogen bond donor, and four hydrophobic features. The most active molecule in the training set fits the pharmacophore model perfectly with the highest scores. The pharmacophore model was further used to screen potential compounds from the Maybridge database followed by virtual screening that produced 14 hits molecules. Then, we used molecular docking methods, as added tools for virtual

screening to visualize binding pose, hydrogen bonding, and π - π stacking with the important residue in the catalytic and peripheral binding site residue viz. TYR121, TRP84, and PHE330. The docked pose of 44 1-indanone derivatives and virtually screened hits also matches the selected pharmacophore. In addition, known active compounds were used for the development of QSAR model to use them to predict activity of the virtually screened compounds. Using a combination of pharmacophore modeling, virtual screening, molecular docking, and QSAR, we successfully identified several new other scaffolds like benzothiazole, benzylpiperazine and benzylpiperidine, pyrazole, piperidine, pyridine and thiazolidine derivatives, etc., that have not been previously characterized in the scientific literature as Alzheimer's AChE inhibitors and can be useful to a medicinal chemist or combinatorial chemist to pick up the new molecular starting points for medicinal chemistry optimization for the design of novel Alzheimer's AChE inhibitors.

Acknowledgments Authors are grateful to French Chemoinformatics Society and Prof. Alexandre Varnek, University of Strasbourg, France for providing the necessary software in 2nd Summer School of Chemoinformatics, Obernai, France, 2010 and Inte:Ligand, GmbH for giving academic license of LigandScout to carry out Pharmacophore screening.

References

- Allen NHP, Burns A (1995) The treatment of Alzheimer's disease. *J Psychopharmacol* 9:43–56
- Bar-On P, Millard CB, Harel M, Dvir H, Enz A et al (2002) Kinetic and structural studies on the interaction of cholinesterases with the anti-Alzheimer drug rivastigmine. *Biochemistry* 41:3555–3564
- Bartolini M, Bertucci C, Cavrini V, Andrisano V (2003) Beta-amyloid aggregation induced by human acetylcholinesterase: inhibition studies. *Biochem Pharmacol* 65:407–416
- Berman HM, Westbrook J, Feng Z, Gilliland G, Bhat TN et al (2000) The protein data bank. *Nucleic Acids Res* 28:235–242
- Bikadi Z, Hazai E (2009) Application of the PM6 semi-empirical method to modeling proteins enhances docking accuracy of AutoDock. *J Cheminform* 1:15
- Bolognesi ML, Andrisano V, Bartolini M, Banzi R, Melchiorre C (2005) Propidium-based polyamine ligands as potent inhibitors of acetylcholinesterase and acetylcholinesterase-induced amyloid-beta aggregation. *J Med Chem* 48:24–27
- Cheng DH, Tang XC (1998) Comparative studies of huperzine A, E2020, and tacrine on behavior and cholinesterase activities. *Pharmacol Biochem Behav* 60:377–386
- Dewar MJS, Zoebisch EG, Healy EF, Stewart JJP (1985) The development and use of quantum mechanical molecular models. 76. AM1: a new general purpose quantum mechanical molecular model. *J Am Chem Soc* 107:3902–3909
- Du DM, Carlier PR (2004) Development of bivalent acetylcholinesterase inhibitors as potential therapeutic drugs for Alzheimer's disease. *Curr Pharm Des* 10:3141–3156
- Ellman GL, Courtney KD, Andres V Jr, Feather-Stone RM (1961) A new and rapid colorimetric determination of acetylcholinesterase activity. *Biochem Pharmacol* 7:88–95
- Francis PT, Palmer AM, Snape M, Wilcock GK (1999) The cholinergic hypothesis of Alzheimer's disease: a review of progress. *J Neurol Neurosurg Psychiatry* 66:137–147
- Friedman JH, Roosen CB (1995) An introduction to multivariate adaptive regression splines. *Stat Methods Med Res* 4:197–217
- Galisteo M, Rissel M, Sergeant O, Chevanne M, Cillard J et al (2000) Hepatotoxicity of tacrine: occurrence of membrane fluidity alterations without involvement of lipid peroxidation. *J Pharmacol Exp Ther* 294:160–167
- Giacobini E, Spiegel R, Enz A, Veroff AE, Cutler NR (2002) Inhibition of acetyl- and butyryl-cholinesterase in the cerebrospinal fluid of patients with Alzheimer's disease by rivastigmine: correlation with cognitive benefit. *J Neural Transm* 109:1053–1065
- Greenblatt HM, Kryger G, Lewis T, Silman I, Sussman JL (1999) Structure of acetylcholinesterase complexed with (–)-galanthamine at 2.3 Å resolution. *FEBS Lett* 463:321–326
- Greig NH, Utsuki T, Yu Q, Zhu X, Holloway HW et al (2001) A new therapeutic target in Alzheimer's disease treatment: attention to butyrylcholinesterase. *Curr Med Res Opin* 17:159–165
- Gupta S, Misra G, Pant MC, Seth PK (2011) Prediction of a new surface binding pocket and evaluation of inhibitors against huntingtin interacting protein 14: an insight using docking studies. *J Mol Model* 17:3047–3056
- Gupta S, Misra G, Pant MC, Seth PK (2012a) Targeting the epidermal growth factor receptor: exploring the potential of novel inhibitor N-(3-ethynylphenyl)-6,7-bis (2-methoxyethoxy) quinolin-4-amine using docking and molecular dynamics simulation. *Protein Pept Lett* 19:955–968
- Gupta S, Misra G, Pant MC, Seth PK (2012) Identification of novel potent inhibitors against Bcl-xL anti-apoptotic protein using docking studies. *Protein Pept Lett* 19
- Harel M, Schalk I, Ehret-Sabatier L, Bouet F, Goeldner M et al (1993) Quaternary ligand binding to aromatic residues in the active-site gorge of acetylcholinesterase. *Proc Natl Acad Sci USA* 90:9031–9035
- Harel MQD, Nair HK, Silman I, Sussman JL (1996) The X-ray structure of a transition state analog complex reveals the molecular origins of the catalytic power and substrate specificity of acetylcholinesterase. *J Am Chem Soc* 118:2340–2346
- Ibach B, Haen E (2004) Acetylcholinesterase inhibition in Alzheimer's disease. *Curr Pharm Des* 10:231–251
- Inestrosa NC, Alvarez A, Perez CA, Moreno RD, Vicente M et al (1996) Acetylcholinesterase accelerates assembly of amyloid-beta-peptides into Alzheimer's fibrils: possible role of the peripheral site of the enzyme. *Neuron* 16:881–891
- Kaur J, Zhang MQ (2000) Molecular modelling and QSAR of reversible acetylcholinesterase inhibitors. *Curr Med Chem* 7:273–294
- Kryger G, Silman I, Sussman JL (1999) Structure of acetylcholinesterase complexed with E2020 (Aricept): implications for the design of new anti-Alzheimer drugs. *Structure* 7:297–307
- Labute P (2009) Protonate3D: assignment of ionization states and hydrogen coordinates to macromolecular structures. *Proteins* 75:187–205
- Lee SK, Lee IH, Kim HJ, Chang GS, Chung JE, No KT (2003) The PreADME approach: web-based program for rapid prediction of physico-chemical, drug absorption and drug-like properties, EuroQSAR 2002 Designing drugs and crop protectants: processes, problems and solutions. Blackwell, Boston, pp 418–420
- Lipinski CA, Lombardo F, Dominy BW, Feeney PJ (2001) Experimental and computational approaches to estimate solubility and

- permeability in drug discovery and development settings. *Adv Drug Deliv Rev* 46:3–26
- Mashhadi HR, Shanechi HM, Lucas C (2003) A new genetic algorithm with Lamarckian individual learning for generation scheduling. *IEEE Trans Power Syst* 18:1181–1186
- Morris GM, Huey R, Lindstrom W, Sanner MF, Belew RK et al (2009) AutoDock4 and AutoDockTools4: automated docking with selective receptor flexibility. *J Comput Chem* 30: 2785–2791
- Munoz-Muriedas J, Lopez JM, Orozco M, Luque FJ (2004) Molecular modelling approaches to the design of acetylcholinesterase inhibitors: new challenges for the treatment of Alzheimer's disease. *Curr Pharm Des* 10:3131–3140
- Nachon F, Nicolet Y, Masson P (2005) Butyrylcholinesterase: 3D structure, catalytic mechanisms. *Ann Pharm Fr* 63:194–206
- Parihar MS, Hemnani T (2004) Alzheimer's disease pathogenesis and therapeutic interventions. *J Clin Neurosci* 11:456–467
- Pettersen EF, Goddard TD, Huang CC, Couch GS, Greenblatt DM et al (2004) UCSF Chimera—a visualization system for exploratory research and analysis. *J Comput Chem* 25:1605–1612
- Ravelli RB, Raves ML, Ren Z, Bourgeois D, Roth M et al (1998) Static Laue diffraction studies on acetylcholinesterase. *Acta Crystallogr D Biol Crystallogr* 54:1359–1366
- Raves ML, Harel M, Pang YP, Silman I, Kozikowski AP et al (1997) Structure of acetylcholinesterase complexed with the nootropic alkaloid, (–)-huperzine A. *Nat Struct Biol* 4:57–63
- Rodriguez-Franco MI, Fernandez-Bachiller MI, Perez C, Castro A, Martinez A (2005) Design and synthesis of *N*-benzylpiperidine-purine derivatives as new dual inhibitors of acetyl- and butyrylcholinesterase. *Bioorg Med Chem* 13:6795–6802
- Rucker C, Rucker G, Meringer M (2007) Y-randomisation and its variants in QSPR/QSAR. *J Chem Inf Model* 47:2345–2357
- Savini L, Gaeta A, Fattorusso C, Catalanotti B, Campiani G et al (2003) Specific targeting of acetylcholinesterase and butyrylcholinesterase recognition sites. Rational design of novel, selective, and highly potent cholinesterase inhibitors. *J Med Chem* 46:1–4
- Scarpini E, Scheltens P, Feldman H (2003) Treatment of Alzheimer's disease: current status and new perspectives. *Lancet Neurol* 2:539–547
- Shen Q, Peng Q, Shao J, Liu X, Huang Z et al (2005) Synthesis and biological evaluation of functionalized coumarins as acetylcholinesterase inhibitors. *Eur J Med Chem* 40:1307–1315
- Sheng R, Lin X, Li J, Jiang Y, Shang Z et al (2005) Design, synthesis, and evaluation of 2-phenoxy-indan-1-one derivatives as acetylcholinesterase inhibitors. *Bioorg Med Chem Lett* 15:3834–3837
- Silman I, Sussman JL (2005) Acetylcholinesterase: 'classical' and 'non-classical' functions and pharmacology. *Curr Opin Pharmacol* 5:293–302
- Soreq H, Seidman S (2001) Acetylcholinesterase—new roles for an old actor. *Nat Rev Neurosci* 2:294–302
- Sugimoto H, Yamanishi Y, Iimura Y, Kawakami Y (2000) Donepezil hydrochloride (E2020) and other acetylcholinesterase inhibitors. *Curr Med Chem* 7:303–339
- Veber DF, Johnson SR, Cheng HY, Smith BR, Ward KW et al (2002) Molecular properties that influence the oral bioavailability of drug candidates. *J Med Chem* 45:2615–2623
- Walters WP, Stahl MT, Murcko MA (1998) Virtual screening an overview. *Drug Discov Today* 3:160–178
- Wolber G, Langer T (2005) LigandScout: 3-D pharmacophores derived from protein-bound ligands and their use as virtual screening filters. *J Chem Inf Model* 45:160–169